Chaos, Solitons and Fractals 182 (2024) 114850

Contents lists available at ScienceDirect

Chaos, Solitons and Fractals

journal homepage: www.elsevier.com/locate/chaos

Extending dynamic memory of spiking neuron networks

Vladimir V. Klinshov [a,b], Andrey V. Kovalchuk [a], Igor A. Soloviev [a], Oleg V. Maslennikov [a], Igor Franović [c], Matjaž Perc [d,e,f,g,*]

[a] A.V. Gaponov-Grekhov Institute of Applied Physics of the Russian Academy of Sciences, 46 Ulyanova Street, Nizhny Novgorod, 603950, Russia
[b] National Research University Higher School of Economics, 25/12 Bol'shaya Pecherskaya street, Nizhny Novgorod, 603155, Russia
[c] Scientific Computing Laboratory, Center for the Study of Complex Systems, Institute of Physics Belgrade, University of Belgrade, Pregrevica 118, Belgrade, 11080, Serbia
[d] Faculty of Natural Sciences and Mathematics, University of Maribor, Koroška cesta 160, Maribor, 2000, Slovenia
[e] Community Healthcare Center Dr. Adolf Drolc Maribor, Vošnjakova ulica 2, Maribor, 2000, Slovenia
[f] Department of Physics, Kyung Hee University, 26 Kyungheedae-ro, Dongdaemun-gu, Seoul, 02447, Republic of Korea
[g] Complexity Science Hub Vienna, Josefstädterstraße 39, Vienna, 1080, Austria

ARTICLE INFO

Keywords:
Dynamic memory
Spiking neuron networks
Mean-field model
Reservoir computing

ABSTRACT

Explaining the mechanisms of dynamic memory, that allows for a temporary storage of information at the timescale of seconds despite the neuronal firing at the millisecond scale, is an important challenge not only for neuroscience, but also for computation in neuromorphic artificial networks. We demonstrate the potential origin of such longer timescales by comparing the spontaneous activity in excitatory neural networks with sparse random, regular and small-world connection topologies. We derive a mean-field model based on a self-consistent approach and white noise approximation to analyze the transient and long-term collective network dynamics. While the long-term dynamics is typically irregular and weakly correlated independent of the network architecture, especially long timescales are revealed for the transient activity comprised of switching fronts in regular and small-world networks with a small rewiring probability. Analyzing the dynamic memory of networks in performing a simple computational delay task within the framework of reservoir computing, we show that an optimal performance on average is reached for a regular connection topology if the input is appropriately structured, but certain instances of small-world networks may strongly deviate from configuration averages and outperform all the other considered network architectures.

1. Introduction

Performing various tasks, such as motion coordination and control, speech recognition or driving a car, requires that certain information is temporary stored in the brain for several seconds [1,2]. Nevertheless, the characteristic timescale of neuronal spiking is much faster, namely of the order of milliseconds. The problem of how to accommodate for the gap between these two timescales, such that the information is preserved for times much longer than that of neuronal spiking, has long been in the focus of an intense debate [2–9]. While forming memories on timescales of hours or longer is deemed to be facilitated by synaptic weights, the information on a timescale of several seconds is likely stored in the activity patterns. A rather obvious candidate, the working memory, can indeed last for tens of seconds, but its functionality is still limited by the small capacity of typically not more than ten items [10,11]. Revealing the dynamical mechanism that gives rise to a sufficiently long-term memory in networks of fast spiking neurons would not only provide a possible explanation for the way in which the brain operates, but would also indicate new computational paradigms for efficient processing of time-varying signals in neuromorphic artificial systems [12–16].

A popular paradigm for understanding the information processing in the brain is the reservoir computing [17–21]. In this context, neural circuits within the brain are considered as a reservoir, which constitutes a dynamical system demonstrating complex collective behavior. Input signals perturb this dynamics and so project on the high-dimensional space of the system states. These projections can be extracted from the system by a simple linear readout, and a proper selection of the output weights can in principle allow one to perform an arbitrary operation on the input data. An important property of the reservoir is the transient character of the stimulus-induced dynamics which warrants an unambiguous mapping of the input onto the system state and hence the output. However, some of the transient processes may

* Corresponding author at: Faculty of Natural Sciences and Mathematics, University of Maribor, Koroška cesta 160, Maribor, 2000, Slovenia.
E-mail addresses: vladimir.klinshov@ipfran.ru (V.V. Klinshov), franovic@ipb.ac.rs (I. Franović), matjaz.perc@gmail.com (M. Perc).

https://doi.org/10.1016/j.chaos.2024.114850
Received 1 March 2024; Accepted 6 April 2024
Available online 17 April 2024

in principle be quite slow time facilitating the storage of the input for very long times.

In our previous paper [22], we have considered the dynamic memory [23–25] of neural networks with random connectivity, having demonstrated the so-called rate chaos [26–29], an emergent phenomenon reflected in the slow fluctuations of the network firing rates. The underlying long timescales have naturally led to a hypothesis that such processes may be leveraged for longer-term dynamic memory. Nevertheless, achieving the extended temporal memory has surprisingly turned out to be dependent on the particular scenario that gives rise to rate chaos, and moreover, the only effective scenario has involved the slow synaptic kinetics [22]. Slow synapses, however, are neither typical for the brain neural circuits nor are beneficial for neuromorphic computing due to their low energy efficiency. These arguments underline the importance of finding a network architecture that is based on fast synapses and yet supports long-lasting dynamic memory.

We focus on this very problem and demonstrate the properties of optimal network architecture and the input structure that facilitate extended dynamic memory. In particular, we investigate how the lifetime of dynamic memory depends on the network topology, comparing the three paradigmatic cases of random, regular and small-world networks. The spontaneous network dynamics is investigated by developing a mean-field theory [8,9,30–32] based on a white noise approximation, which describes the transient and long-term network behavior in a self-consistent way. The mean-field model is used to explain the origin of characteristic longer timescales that are associated with the propagation of network activity following a spatially and temporally localized excitation, and are an important ingredient in developing sufficiently long dynamic memory. We show that the small-world architecture provides an optimal substrate for episodic memory tasks in case of a homogeneously distributed input. Nevertheless, introducing a spatially structured input substantially improves the performance of regular networks, making them superior to the small-world networks. Surprisingly, we also reveal that there may exist particular small-world network configurations for intermediate rewiring probabilities that perform substantially better than the respective averages and even outperform all the other considered network topologies.

The paper is organized as follows. In Section 2, we introduce the model of a network of excitatory theta neurons with double exponential synapses. In Section 3, we focus on the networks with the sparse random topology, and develop a mean-field model of collective dynamics, showing that it may explain both the transient and the long-term network dynamics. In Sections 4 and 5, the mean-field theory is generalized to regular ring and small-world networks, pointing out the differences in their respective transient dynamics and explaining the mechanisms of localized correlated fluctuations that give rise to longer characteristic timescales. In Section 6, we analyze how the ability of a network to perform a simple computational delay task depends on the network topology, indicating the network architecture and the input structure optimal for extended dynamic memory. Section 7 provides a summary of our main findings.

2. Model

Our model is a network of N theta neurons [33,34] whose isolated dynamics is given by

$$\frac{d\theta}{dt} = (1-\cos\theta) + (1+\cos\theta)I, \tag{1}$$

where $\theta \in S^1$ is the phase variable describing the state of the neuron, whereas I denotes an external stimulation current. Note that the phase is related to the membrane voltage by $V = \tan(\theta/2)$ [35,36], such that (1) may be rewritten in an equivalent form

$$\frac{dV}{dt} = V^2 + I, \tag{2}$$

yielding the classical quadratic integrate-and-fire neuron model [37, 38]. Nevertheless, the latter is inconvenient for simulation because the spiking event conforms to V_j reaching infinity, so we prefer to use the theta-neuron representation where the neuron fires a spike once its phase crosses the threshold $\theta = \pi$.

The dynamics of a theta neuron is controlled by the input current I. If the latter is constant, a neuron can either be in the excitable ($I < 0$) or the oscillatory ($I > 0$) regime, which are separated by the saddle–node of infinite period (SNIPER) bifurcation at $I = 0$. In the excitable regime, which is important to our subsequent analysis, a neuron possesses the stable rest state $\theta = -\arccos((1+I)/(1-I))$ and an unstable stationary state $\theta = \arccos((1+I)/(1-I))$. The latter provides for the excitation threshold: if a perturbation applied to the neuron shifts its phase above this threshold, the neuron performs a revolution crossing the $\theta = \pi$ value to emit a spike. Following the spike, the neuron returns back to its resting state. Note that the distance between the resting state and the excitation threshold decreases as $\sqrt{-I}$ when the input I tends to zero (from below), so that for small negative inputs the neuron becomes highly susceptible to external perturbations.

When embedded into a network, the neurons $j = 1, \dots, N$ receive the input currents

$$I_j = I_b + g\sum_{k=1}^{N} A_{jk} r_k. \tag{3}$$

comprised on an external (slightly negative) constant bias current I_b and the synaptic current. Within the latter term, g is the coupling coefficient, A_{jk} are the elements of the coupling matrix determining the structure and the strength of synaptic connections, and r_k are the synaptic output currents obeying the second order kinetics:

$$\frac{dr_j}{dt} = -\frac{r_j}{\tau_d} + h_j, \tag{4}$$

$$\frac{dh_j}{dt} = -\frac{h_j}{\tau_r} + \frac{1}{\tau_r\tau_d}\sum_{t_j^p}\delta(t-t_j^p). \tag{5}$$

Eqs. (4) and (5) describe the double exponential synapses [39], where the parameters τ_r and τ_d denote the synaptic rise and decay times which respectively account for the rapid binding and slow unbinding of neurotransmitters, while t_j^p are the firing times of neuron j.

3. Sparse random network

Collective dynamics of the network strongly depends on its structure given by the adjacency matrix A_{jk}. Let us begin by considering an Erdos–Rényi network with the connectivity $c = 0.1$, so that the elements of the adjacency matrix are set to be nonzero with the given probability c, see the coupling matrix in Fig. 1(a). The weights of the nonzero connections are drawn randomly from the Gaussian distribution with zero mean and variance $(Nc)^{-1}$. Then each neuron has on average Nc incoming connections with zero mean and the variance $g^2(Nc)^{-1}$. Since the fraction of shared connections between any two neurons is small due to the network sparseness, it is reasonable to assume that the firing of the neurons is weakly correlated. Thus, each neuron receives a sum of a large number of weakly correlated pulse trains multiplied by random weights which can be approximated by white noise.

To better understand the network dynamics, we first summarize the behavior of a neuron driven by such a noisy signal filtered by the synaptic kinetics (4), (5). If the noise is too weak, the neuron cannot exceed the excitation threshold. For moderate noise, such excitations eventually occur, resulting in occasional spikes. Stronger noise excites the neuron almost immediately after it regains the rest state following the previous spike, which makes the firing more frequent and regular. These points are illustrated in Fig. 2(a) and (b) showing the mean firing rate and the coefficient of variation of inter-spike intervals in dependence of the noise level (note the logarithmic scale on the horizontal axis in Fig. 2(b) and both axis in Fig. 2(a)).

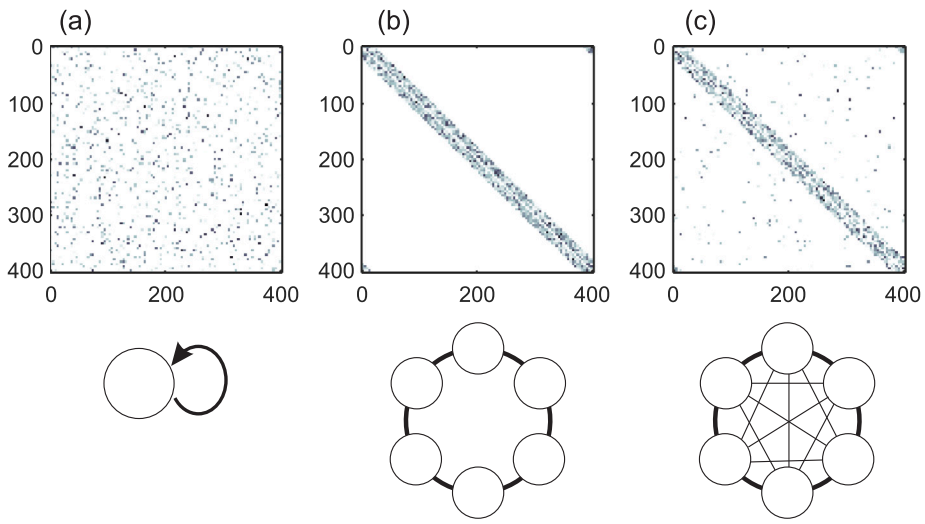

Fig. 1. Top row: coupling matrices for (a) a sparse random network, (b) a regular circular network and (c) a small-world network. Bottom row: representations of the networks as mean-field models. White circles denote neural masses, while black lines denote connections between them. In (b) and (c), self-connections are not shown. In (c), the width of the line is proportional to the coupling strength.

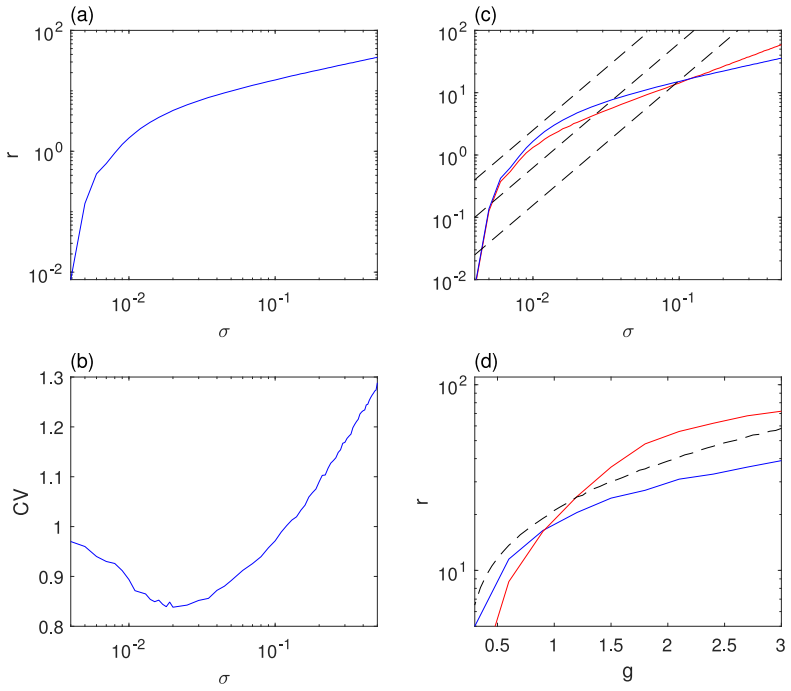

Fig. 2. (a) Mean firing rate of a single neuron in terms of the noise intensity σ. (b) The coefficient of variation of the inter-spike intervals versus the noise intensity. (c) The l.h.s (solid lines) and the r.h.s (dashed lines) of Eq. (6). The r.h.s. is plotted for actual CV (red line) and for $CV = 1$ (blue line). The l.h.s. is plotted for $g = 0.2$, $g = 0.4$ and $g = 0.8$ (top to bottom). (d) Mean firing rate of a random sparse network predicted theoretically from the white noise approximation (solid lines) and obtained by direct numerical simulations (dashed line). Theoretical results are plotted for actual CV from (b) (red line) and for $CV = 1$ (blue line). Parameters: $N = 400$, $c = 0.1$, $\tau_r = 2$, $\tau_d = 20$, $I_b = -0.001$. (For interpretation of the references to color in this figure legend, the reader is referred to the web version of this article.)

Given the insights above, let us now consider the collective network dynamics. If the neurons of the network receive noisy signals of intensity σ and fire irregularly with the mean rate $r = R(\sigma)$, the output produced by all the synapses of a typical neuron can be estimated as a white noise with intensity $\sigma' = CV g\sqrt{r}$, where CV is the coefficient of variation. Thus, the possible collective regimes of the random sparse network are given by the self-consistency conditions

$$CV^2(\sigma)R(\sigma) = \sigma^2/g^2. \tag{6}$$

The left (l.h.s) and right hand sides (r.h.s.) of Eq. (6) are plotted in Fig. 2(c). The l.h.s. is provided in two variants, namely using the actual CV (red curve) and under the approximation of $CV = 1$ (blue curve). The r.h.s. is shown for three different values of the coupling constant g (dashed lines). Due to the logarithmic scale on both axis, the r.h.s. for different g appear as straight lines in descending order with g. For the weak coupling $g = 0.2$, there is no intersection between the curves representing the dependencies on the l.h.s. and r.h.s. of Eq. (6), implying that the network does not support self-sustained activity. Note that the silent state where all the neurons are at rest is always stable because the isolated neurons are excitable rather than oscillatory. For sufficiently large $g = 0.4$, cf. the middle dashed line in Fig. 2(c), one finds two intersection points that correspond to self-sustained network activity: an unstable one with the lower activity and a stable one with higher activity. Further enhancing g, see the bottom dashed line ($g =$

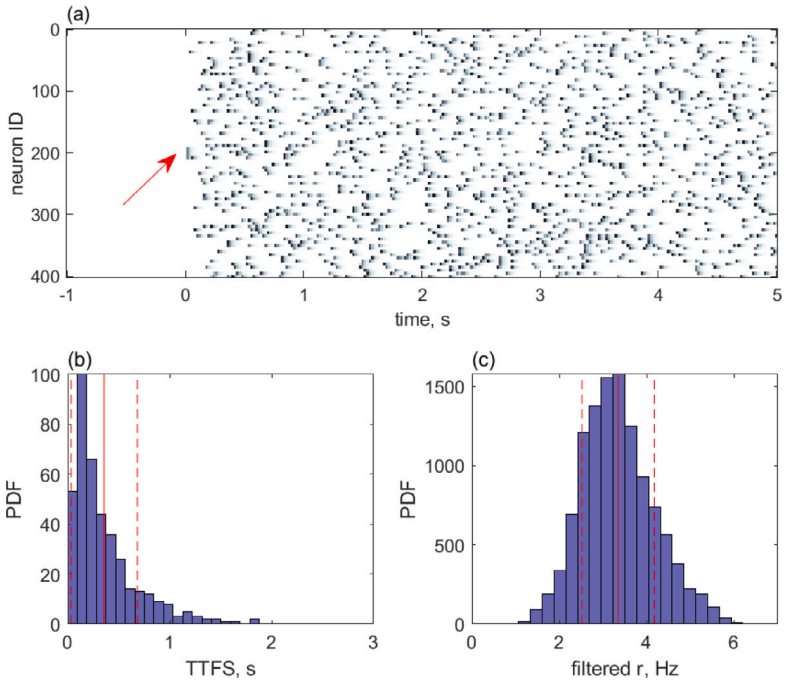

Fig. 3. Local structure of the state with self-sustained activity in a random sparse network. (a) Spike raster plot; red arrow: moment and locus of the applied external input. (b) Distribution of the times to first spike (TTFS). (c) Distribution of the spatially and temporally filtered neural activity. In (b) and (c), red solid vertical lines denote the means of the distributions, whereas the dashed lines indicate the means plus/minus the standard deviation. Parameters: $N = 400$, $c = 0.1$, $\tau_r = 2$, $\tau_d = 20$, $I_b = -0.001$, $g = 0.3$. (For interpretation of the references to color in this figure legend, the reader is referred to the web version of this article.)

0.8), the network mean rate increases, as corroborated by the shift of the top intersection point to the right.

In this way, the response of a single neuron to white noise allows one to predict the collective regimes of a sparse random network. To validate the above predictions, we have compared them to the results of direct numerical simulations of a random sparse network, considering averaging time intervals of 100 s for a set of different g values varying between 0 and 3. To avoid trapping into the silent state, the network has to be stimulated by a brief strong input which allows it to settle to the regime of self-sustained activity. Fig. 2(d) shows the dependencies of the network mean firing rate obtained from the simulations and from Eq. (6) on the coupling strength g. The self-consistency results are plotted using the actual CV (red curve) and the Poisson approximation $CV = 1$ (blue curve).

In Fig. 3(a) is shown the spike raster plot illustrating the local structure of a typical state featuring collective self-sustained activity. The network is activated at $t = 0$ by a strong stimulus applied to 10 neurons with indices $j = 201$ to $j = 210$, cf. the red arrows. Note that the activity rapidly spreads across the network. To demonstrate this, we have plotted the distributions of the times to first spike (TFTS) in Fig. 3(b). One finds that the neurons fire for the first time in 0.36 ± 0.32 s after the network activation. After encompassing the whole network, the activity remains irregular and distributed homogeneously both in space and time. To corroborate the homogeneity feature, we have filtered the network activity taking the moving average both in time (averaging time interval of 0.5 s) and in space (averaging over the spatial window of 20 neurons assuming that the neurons lie on a ring with periodic boundary conditions). The distribution of the filtered activity in Fig. 3(c) turns to be relatively narrow with the mean 3.35 and standard deviation 0.83 which gives the coefficient of variation $CV = 0.25$.

Numerical simulations of the network activity together with the self-consistency theory allows one to formulate the mean-field or a neural mass model of the dynamics of a random sparse network. Since its activity is homogeneous, it can be described by the single variable $r = \frac{1}{N}\sum_{j=1}^{N} r_j$ which presents the mean synaptic output of all the neurons. In particular, the latter obeys

$$\frac{dr}{dt} = -\frac{r}{T} + R(g\sqrt{r}), \tag{7}$$

where $T = 0.36$ s is the characteristic time of the activity onset estimated as the mean of TTFS, $R(\sigma)$ is the firing rate of a single neuron receiving noisy input of the intensity σ, and σ is the intensity of the effective noise received by the neurons of the network with the activity r. For the Poisson approximation $CV = 1$, the effective noise intensity may be written as $\sigma = g\sqrt{r}$.

The dynamics of the mean-field model (7) is rather simple: for strong enough coupling, it has two steady state, namely the silent one with $r = 0$ and the active one with r given by the self-consistency condition (6). These two states are separated by an unstable steady state serving as an excitation threshold. If the external stimulus takes the system over the threshold, its dynamics settles into the active state following the transient of duration T. Thus, the mean-field model captures well the dynamics of a random sparse network. In the following, we will show that this mean-field model can be useful for describing the activity networks with other connectivity patterns.

4. Regular ring network

In this Section, we consider a network with regular ring topology so that two neurons i and j are connected if and only if $|i - j| \le m$ where m is a positive integer, cf. the corresponding coupling matrix in Fig. 1(b). To keep the total number of connections per neuron equal to the previously considered case of a random network we take $m = cN/2$. The connection weigths are again drawn from the Gaussian distribution with zero mean and variance $(Nc)^{-1}$, so that the variance of the incoming connection weights is again the same as for the random network. However, now each neuron is connected only with its neighbors rather than the whole network, which results in the emergence of novel dynamical features.

The typical dynamics of a regular ring network is illustrated by the spike raster plot in Fig. 4(a). As in Fig. 3(a), we activated the network

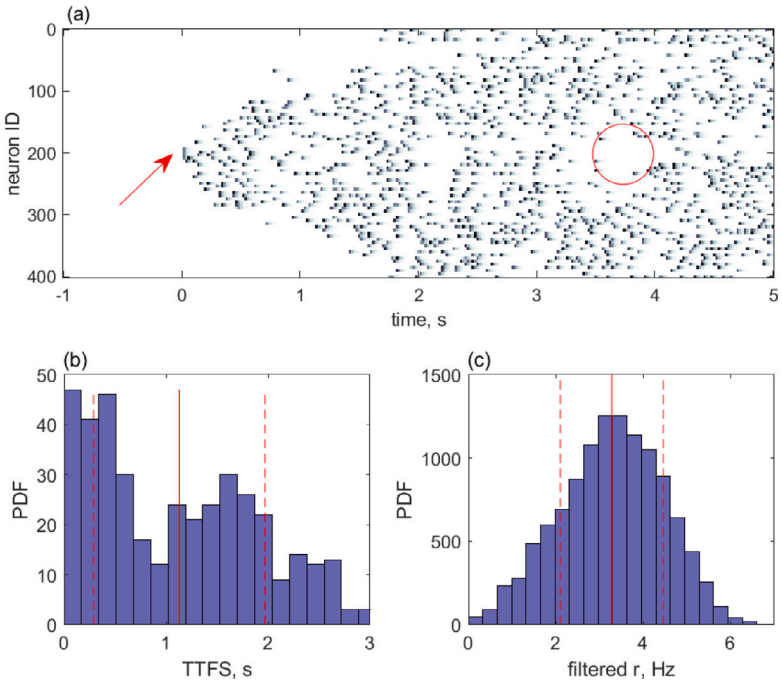

Fig. 4. Local structure of self-sustained activity in a regular ring network. (a) Spike raster plot; red arrow: moment and locus of the external input; red circle: moment and locus of the correlated activity collapse. (b) Distribution of times to first spike (TTFS). (c) Distribution of spatially and temporally filtered neural activity. In (b) and (c), red solid vertical lines denote the means of distributions, while dashed lines indicate means plus/minus standard deviation. Parameters: $N = 400$, $m = 20$, $\tau_r = 2$, $\tau_d = 20$, $I_b = -0.001$, $g = 0.3$. (For interpretation of the references to color in this figure legend, the reader is referred to the web version of this article.)

by applying a strong stimulus to 10 neurons at $t = 0$ (red arrow). However, here the activity spreads across the network gradually due to absence of long-range connections. As evident from the spike raster plot, it takes about 2 s for the activity to spread across the entire network. This property is reflected in the distribution of the TTFS in Fig. 4(b), which reveals that the neurons fire for the first time at $t = 1.13 \pm 0.84$ s. This characteristic timescale of transient processes of about 1–2 s may play an important role for the dynamic memory of the network.

Moreover, even after encompassing the whole network, the activity turns out to be less homogeneous than for the random network. This heterogeneity manifests itself through recurrent events of correlated collapses of local activity, see the example of a white spot marked by a red circle in Fig. 3(a). To quantify the heterogeneity of the network activity, we have filtered the network activity both in space and time, using the method described in Section 3. The distribution of the filtered activity much wider than for the random sparse network, featuring the mean of 3.28, standard deviation of 1.18 and the CV = 0.36, see Fig. 4(c). Note that the distribution of the filtered activity spans down to zero reflecting the localized activity collapses. Thus, the sustained dynamics of the network is also enriched with a new time scale of about 0.5 s which may as well be important for the realization of the dynamic memory.

To explain the dynamics of a regular ring network via the mean-field model, we approximate it as a ring of subnetworks of size m resided on a ring where each subnetwork is connected only to its two nearest neighbors. Then, each subnetwork receives half of its connections from within, and a quarter of connections from each neighboring subnetwork, see Fig. 1(b). The mean-field model (7) can be adapted to describe the dynamics of a single subnetwork if the input into this subnetwork is calculated as a sum of the inputs from itself and both neighbors. Then the dynamics of the whole network is governed by

$$\frac{dr_j}{dt} = -\frac{r_j}{T} + R\left(g\sqrt{\frac{r_j}{2} + \frac{r_{j-1}}{4} + \frac{r_{j+1}}{4}}\right), \tag{8}$$

where r_j is the activity of the jth subnetwork, having inherited the periodic boundary conditions. System (8) presents a ring of $n = N/m$ units with bidirectional local coupling. Since each node is a bistable unit, the propagation of switching fronts along the ring is possible: when one of the units is switched into the active state, it excites its neighbors forcing them to switch to the active states as well, and so on. To estimate the time that takes to switch the whole network into the active state, recall that a single unit has a typical switching (excitation) time T, and since the switching front propagates in both directions, the total time equals

$$T_\Sigma = \frac{n}{2}T = \frac{T}{c}. \tag{9}$$

For our parameters, the estimate gives $T_\Sigma = 3.6$, which is in good agreement with the results of numerical simulations from Fig. 4(b) where some of the neurons fire for the first time not earlier than 3 s after the excitation of the activity seed.

5. Small-world network

We have demonstrated that the transient collective dynamics of a regular network features longer timescales compared to the random sparse network. The longest timescale is associated with the propagation of the excitation fronts along the ring and can be estimated as being $1/c$ times larger than that of a random network. To explain the mechanism giving rise to this longer timescale, we now focus on the transition between the random and the regular network topology. In particular, we invoke the model of small-world networks [40] whose connectivity structure may interpolate between the regular and random networks. Small-world networks are characterized by a short average path length between any two nodes (like random networks) and yet high clustering coefficients (like regular networks). They are known to often display optimal dynamical and computational properties, and what proves to be of special interest to our study, have already been indicated as potential substrates for long-term memory [41].

To obtain the small-world connectivity matrix, we follow the classical algorithm from Watts and Strogatz [40]. Namely, starting from the regular ring network, we randomly rewire each connection with a given probability p and leave it untouched with the probability $1 - p$.

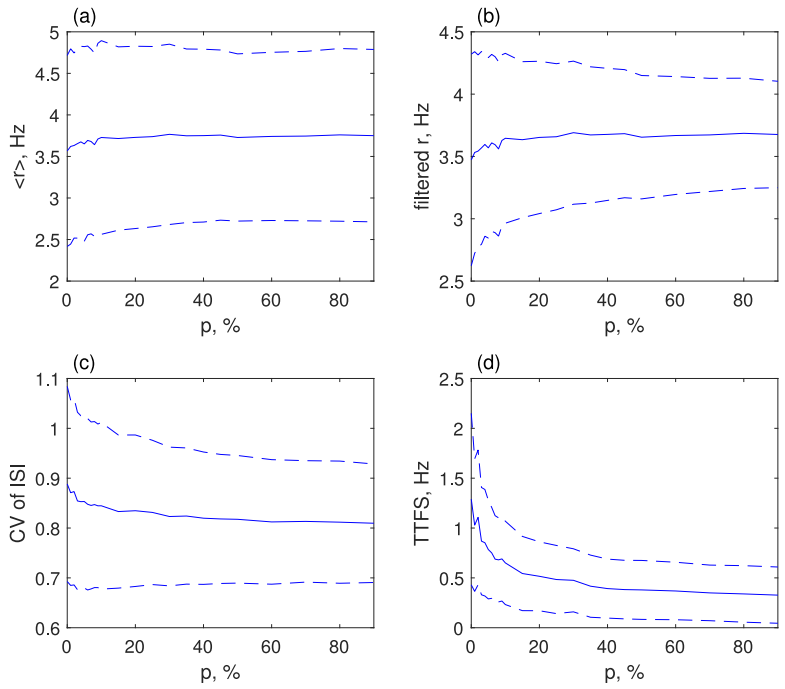

Fig. 5. Quantitative measures of the collective dynamics of a small-world network in terms of the rewiring probability p. (a) Mean firing rate $\langle r\rangle$ of individual neurons. (b) Spatially and temporally filtered activity. (c) Coefficients of variation (CV) of inter-spike intervals. (d) Times to first spike (TTFS). All the results are obtained by averaging over an ensemble of 50 different network realizations. Parameters: $N = 400$, $c = 0.1$, $\tau_r = 2$, $\tau_d = 20$, $I_b = -0.001$, $g = 0.3$.

Choosing different values of p allows one to interpolate between regular networks ($p = 0$) and random networks ($p = 1 - c$).

Next we show that the dynamics in small-world networks can also be described in terms of an appropriate mean-field model. To do so, we again divide the network into subnetworks of size m, but in contrast to the case of regular networks, for any $p > 0$, each subnetwork is connected to all the other subnetworks. Then the fractions of connections received from different subnetworks are given by

$$\alpha_s = \frac{1-p}{2} \quad \text{for self-connections,}$$
$$\alpha_n = \frac{1-c-(1-2c)p}{4(1-c)} \quad \text{for connections from the neighbors,}$$
$$\alpha_o = \frac{pc}{2(1-c)} \quad \text{for connections to the other subnetworks.}$$

Thus, the dynamics of the entire network is described as follows:

$$\frac{dr_j}{dt} = -\frac{r_j}{T} + R\left(g\sqrt{\alpha_s r_j + \alpha_n(r_{j-1}+r_{j+1}) + \alpha_o \sum_{k\neq j,j-1,j+1} r_k}\right). \tag{10}$$

Note that the mean-field model (10) predicts that the emergent self-sustained activity of the small-world network should be independent on the rewiring probability p. One may readily verify this by noting that if $r_j = r$ for each j, Eq. (10) transforms into Eq. (7). However, the speed of the activity spreading across the small-world network cannot be readily estimated from the mean-field model and requires numerical simulations.

We have carried out extensive numerical experiments with small-world networks having varied the rewiring probability p from 0 to $1-c$. For each value of p, we generated 50 instances of the coupling matrix. For each coupling matrix, the network activity has first been initiated by exciting 10 adjacent neurons, and has then been monitored for the next 10 s. For every trial, we have calculated the following measures: (i) distributions of the mean firing rates of individual neurons, (ii) distributions of temporally and spatially filtered activity, (iii) distributions of coefficients of variation of inter-spike intervals of individual neurons, and (iv) distributions of TTFS. For each of these distributions, we have calculated the mean and the variance, having further averaged them across the trials, see the results in Fig. 5.

As predicted by the mean-field theory, the average network activity does not depend on the rewiring probability and remains very close to $\langle r\rangle = 3.7$ for all values of p. As for the filtered activity, its mean is naturally close to this value, but the deviations are more pronounced for smaller p, i.e. closer to the limit of regular networks. This reflects the possibility of strong correlated fluctuations of local activity with typical timescales of about 500 ms (the width of the window of the temporal filter). This is also corroborated by the larger coefficients of variation of the inter-spike intervals for small p. Nevertheless, the most striking feature of the networks with small p is the slow propagation of activity across the network which gives rise to large TTFS that may even span several seconds. One may assume that the emergence of this slowest timescale may provide the basis for comparably long dynamic memory. This conjecture is investigated in Section 6, considering how the networks with different rewiring probability p perform computational tasks requiring episodic memory.

6. Dynamic memory of the network

Performing computations by the neural network involves receiving the input signals, responding to them through intrinsic network dynamics and sending output that reflects the results of information processing. Having the network perform certain computational tasks is achieved by its training. Here we use the framework of reservoir computing [17,42], a concept rooted in liquid-state and echo-state machines [20,43]. This method considers the neural network as a "reservoir" and entails training of output connections only, leaving the network intrinsic structure untouched [18]. This allows not only for an efficient and fast training, but also enables one to relate the performance of various networks with their structure and compare the different network configurations in terms of their computational efficiency.

We have trained the network to perform the following simple computational delay task. An input signal comprising a Poisson spike train with the rate $\lambda = 1$ Hz is presented to the network, and the network has

to recall whether it has received a spike or not within the given past period. In particular, there is a certain interval τ, such that the network is expected to respond by "1" if it has received at least one spike within the last τ milliseconds and by "0" otherwise. Obviously, the network performance depends crucially on the value of the delay τ which is the key parameter of the task. The maximal delay for which the network demonstrates a sufficient accuracy provides a reasonable estimate for the duration of its dynamic memory.

The input signal is fed into the network by adding it to the signal received by each neuron, so that (3) modifies to

$$I_j = I_b + g\sum_{k=1}^{N} A_{jk} r_k + g_{inp} u_j r_{inp}. \tag{11}$$

where g_{inp} is the input gain, u_j are the input weights for the neurons, and r_{inp} is the input synaptic current derived from filtering of the input signal by the same type of synaptic kinetics as within the network:

$$\frac{dr_{inp}}{dt} = -\frac{r_{inp}}{\tau_d} + h_{inp}, \tag{12}$$

$$\frac{dh_{inp}}{dt} = -\frac{h_{inp}}{\tau_r} + \frac{1}{\tau_r \tau_d}\sum_{t_{inp}^p} \delta(t - t_{inp}^p), \tag{13}$$

where t_{inp}^p are the moments of the input spikes. The output of the network is calculated as

$$r_{out} = \sum_{j=1}^{N} w_j r_j, \tag{14}$$

where w_j are the output weights which are to be tuned during the training. The network response is assumed to be "1" if its output exceeds a certain threshold θ and "0" otherwise. The choice of θ allows for the trade-off between the false positive and false negative rates.

We have used the method of least squares [44] to train the output weights during a training period t_{train}, after which the network's performance was estimated during a test period $t_{test} = 100$ s. To characterize the performance, we introduce the error in the same way as in our previous work [22]

$$\varepsilon = \varepsilon_0 \mathrm{fnr} + \varepsilon_1 \mathrm{fpr}, \tag{15}$$

where fpr and fnr respectively denote false positive rate and false negative rate, and ε_0 and ε_1 are the error weights set such that a constant output of either zero or one leads to a total error $\varepsilon = 1$. The network performance P is then estimated as the inverse of the error $P = 1/\varepsilon$.

Following our previous paper [22], we have used the training time of $t_{train} = 100$ s and $g_{inp} = 10$ in all the numerical experiments considered below. We generated a set of networks with coupling matrices A obtained with different rewiring probabilities p varying from 0 to $1 - c$. For each p we have generated ten instances of the network. Having trained each network to solve the delay task for different τ, we have plotted for each p the configuration-averaged performance P as a function of the delay τ. For each p the resultant plot turned out to be unimodal with optimal performance found for intermediate delays. Low performance at small delays is the result of inertness of the neurons which cannot react immediately to a stimulus, while the decay of the performance at large delays is due to the forgetting of the input with time. Thus, the delay values corresponding to optimal performance provide a reasonable estimate of the memory duration.

Nevertheless, it turns out that the memory lifetime substantially depends on the configuration of the input weights. Let us first consider the standard homogeneous input scheme where the input weights are drawn randomly from a uniform distribution $u_j \in [-1; 1]$. The corresponding performance curves are provided in Fig. 6(a). Surprisingly, the results have shown almost no dependence on p for $p > 0$ which has allowed us to present the averaged results for all $p > 0$. The performance of a regular network with $p = 0$ is only marginally better than the average performance of small-world networks.

However, the difference between regular and small-world networks dramatically increases when the input weight configuration is modified so to obtain a spatial structure. To do so, we have reordered the earlier generated coupling weights such that all the positive weights project onto one half of the neurons with indices $j = 101$ to $j = 300$ and the negative weights are supplied to the rest of the network. Such reordering almost mkes no impact on the performance of small-world networks with $p > 0$ but significantly improves the performance of the regular network ($p = 0$). The reason is the interaction of the input weights structure with the ordered spatial structure of the regular network. Due to the presence of these two structures, an input pulse triggers excitation in one half of the network and inhibits the activity in the other half. Then in a regular ring network, it takes a certain time for the activity to spread over the entire network, and this time represents the lifetime of the dynamic memory.

The enhancement of the memory lifetime turns to be even stronger when the input weights are more structured. To showcase this, we introduce positive weights only for the 10% of adjacent neurons with $j = 181$ to $j = 220$ and negative for the other ones, having rescaled the weights to preserve their mean and variance. Then the input pulse inhibits 90% of the network, and it takes even more time for the activity to reverberate in a regular network. As a result, the memory lifetime increases even more. Interestingly, in small-world networks, focusing of the positive input to only 10% of neurons also yields a moderate improvement of the network performance. The likely reason is the effective increase of the input gain g_{inp} which is already known to influence the network computational capabilities [22].

The results so far seem to suggest that regular networks are optimal in terms of dynamic memory lifetime, and any rewiring, even a weak one ($p = 0.01$), deteriorates the performance due to violating the network's regular spatial structure. However, a more in-depth study of the consistency of network performance for different configurations with the same p reveals a more complicated picture. As an example, the performances curves of five different networks with $p = 0$ and $p = 0.09$ are plotted in Fig. 6(b). For the regular network the performance curves follow each other quite closely, while for the small-world network most of the curves do the same with a remarkable exception of one curve lying much higher than the others. Detailed investigation shows that such strong deviations occur rarely but regularly for small-world networks with intermediate rewiring probabilities.

To demonstrate that, we calculated the average and maximal performances at a certain large delay value $\tau = 700$ for 30 instances of coupling matrix generated with different values of p. The results in Fig. 7 refer to the homogeneous input weights. Although the average performance is almost independent on p, the maximal performance demonstrate a pronounced peak at $p = 0.09 \div 0.1$. Note that the standard deviation of the performance for such p does not show a substantial growth which implies that the configurations with extended dynamical memory are not typical, yet emerge regularly (1–2 instances out of 30).

7. Discussion and conclusions

We have considered the collective behavior and the formation of dynamic memory in excitatory spiking neural networks with random, regular ring and small-world connection topologies. To get an insight into the collective regimes, we have developed a mean-field model approximating the input as white noise, which allowed us to describe the network activity in a self-consistent way by the average firing rate. Though derived for the case of sparse random topology, the mean-field model turned out to be useful in explaining the collective dynamics for other network topologies, combined with extensive numerical simulations.

In terms of autonomous dynamics, the properties of all three network types are relatively close. Namely, they all show irregular, weakly correlated activity of individual neurons with coefficient of variation of inter-spike intervals close to one. A certain distinction of regular

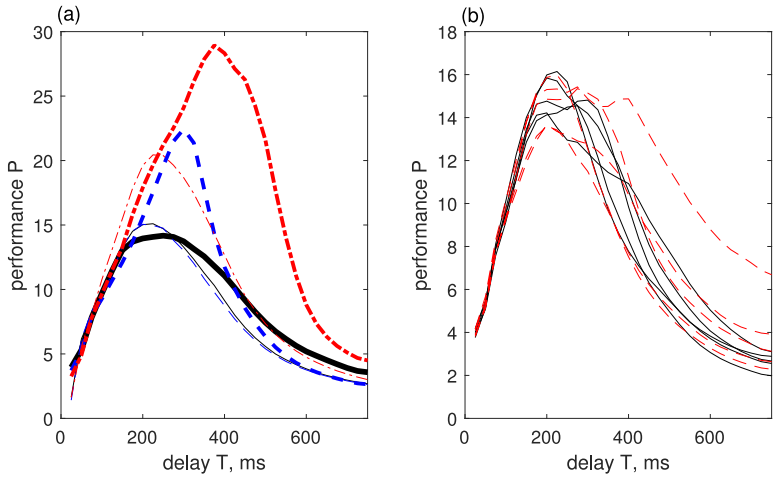

Fig. 6. Network performance P in dependence of delay τ. (a) Performance averaged over 30 network configurations with the same value of p. Black solid curves: homogeneous input weights, blue dashed curves: positive input weights projecting on half of the network, red dashed–dotted curves: positive input weights focused on 10% of the network. Thin curves: averaged data for $p > 0$, thick curves: data for $p = 0$ (regular network). (b) Performance of single configurations of the networks with $p = 0$ (black solid curves) and $p = 0.09$ (red dashed curves) for homogeneous input weights. (For interpretation of the references to color in this figure legend, the reader is referred to the web version of this article.)

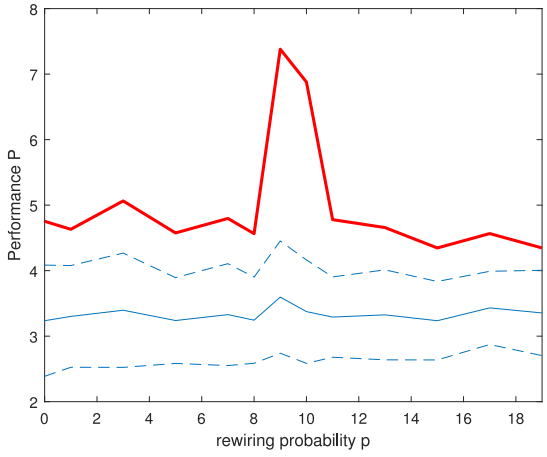

Fig. 7. Performance P of 30 instances of the small-world network in terms of rewiring probability p. Blue solid line: average performance, blue dashed lines: average plus/minus standard deviation, red thick solid line: maximal performance. (For interpretation of the references to color in this figure legend, the reader is referred to the web version of this article.)

networks and small-world networks with weak rewiring is the recurrent emergence of spatially and temporally correlated fluctuations of local activity which, however, are relatively rare. In contrast to long-term dynamics, the transient dynamics depends strongly on the rewiring probability p. The most striking difference concerns the character of the activity spreading over the network after introducing a localized excitation. For random networks (and small-world networks with large $p > 0.1$) the spreading process is fast, taking less than a second. For regular networks (and small-world networks with small $p < 0.1$), the activity spreading resembles the propagation of a switching front and may take up to several seconds. This property endows the network dynamics with slow timescales which can provide the substrate for prolonged dynamic memory.

The dependence of the dynamic memory on the network connectivity patterns has been investigated by training the networks to perform a simple computational task requiring the temporary storage of information for a certain period τ. In this scenario, the maximal time for which the system performance remains high provides a reasonable estimate for the memory duration. We have shown that the average performance of a small-world network depends only marginally on the rewiring probability in a wide range of $p \in [0.01, 0.9]$. For all such networks, the maximal performance $P \approx 15$ is reached at $\tau \sim 200 \div 250$ ms. This implies that on average, the small-world networks facilitate similar dynamic memory as random networks.

We have further demonstrated that, in contrast to small-world networks, the performance of regular networks crucially depends on the structure of input weights feeding the input signal. For a homogeneous distribution of input weights, the average performance of regular networks is very close to that of small-world networks. However, when the positive (excitatory) weights are focused on a localized part of the network, the regular networks start to outperform small-world ones with the maximal performance reached at $\tau \approx 300$ ms when the positive input is applied to 50% of neurons, and at $\tau \approx 350 \div 400$ ms when it projects to 10% of neurons. The performance $P \approx 15$ is reached for $\tau \approx 550$ ms which corresponds to almost tripling of the memory lifetime compared to small-world networks. Extension of the dynamic memory duration in regular networks is apparently related to the fact that their spatial structure allows for the propagation of activity wavefronts across the network, conveying the information about the input for relatively long times. In other words, to utilize the network structure, the input to the network has to be structured as well. Consistent with [2], we have found that random networks are least suitable for dynamic memory tasks.

Considered *on average*, the transition from regular to small-world networks appears destructive for the memory lifetime. Indeed, even a weak rewiring of the connections with the probability as small as 1% reduces the memory performance to that of a random network. Obviously, the rewiring violates the regularity of the network structure and prevents one from using it for prolonged data storage. However, a more detailed study has revealed that for intermediate rewiring probabilities $p \sim 0.1$, *some* network configurations may still demonstrate an extended dynamic memory, even outperforming the regular networks for long delays τ. This implies that certain realizations of random rewiring may be more favorable for temporary data storage than others. Intriguing questions for future study are to understand why there are such preferred configurations and to develop algorithms that would allow one to generate them in a controlled way.

CRediT authorship contribution statement

Vladimir V. Klinshov: Conceptualization, Data curation, Formal analysis, Funding acquisition, Investigation, Methodology, Project administration, Resources, Software, Supervision, Validation, Visualization, Writing – original draft, Writing – review & editing. **Andrey V.**

Kovalchuk: Conceptualization, Data curation, Formal analysis, Investigation, Methodology, Resources, Software, Supervision, Validation, Visualization, Writing – original draft, Writing – review & editing. **Igor A. Soloviev:** Resources, Software, Supervision, Validation, Visualization, Writing – original draft, Writing – review & editing, Conceptualization, Data curation, Formal analysis, Investigation, Methodology. **Oleg V. Maslennikov:** Conceptualization, Data curation, Formal analysis, Investigation, Methodology, Resources, Software, Supervision, Validation, Visualization, Writing – original draft, Writing – review & editing. **Igor Franović:** Conceptualization, Data curation, Formal analysis, Investigation, Methodology, Resources, Software, Supervision, Validation, Visualization, Writing – original draft, Writing – review & editing. **Matjaž Perc:** Conceptualization, Data curation, Formal analysis, Investigation, Methodology, Project administration, Resources, Software, Supervision, Validation, Visualization, Writing – original draft, Writing – review & editing.

Declaration of competing interest

The authors declare that they have no known competing financial interests or personal relationships that could have appeared to influence the work reported in this paper.

Data availability

Data will be made available on request.

Acknowledgments

The work on Sections 3, 5 and 6 was supported by the Russian Science Foundation, Grant No. 19-72-10114. The work on Section 4 was supported by the Russian Science Foundation, Grant No. 23-72-10088.

References

[1] Murray J, Bernacchia A, Freedman D, et al. A hierarchy of intrinsic timescales across primate cortex. Nature Neurosci 2014;17:1661. http://dx.doi.org/10.1038/nn.3862.

[2] Wallace E, Maei HR, Latham PE. Randomly connected networks have short temporal memory. Neural Comput 2013;25:1408. http://dx.doi.org/10.1162/NECO_a_00449.

[3] Lim S, Goldman M. Balanced cortical microcircuitry for maintaining information in working memory. Nature Neurosci 2013;16:1306. http://dx.doi.org/10.1038/nn.3492.

[4] Okun M, Steinmetz NA, Lak A, Dervinis M, Harris KD. Distinct structure of cortical population activity on fast and infraslow timescales. Cereb. Cortex 2019;29:2196. http://dx.doi.org/10.1093/cercor/bhz023.

[5] Ho ECY, Strüber M, Bartos M, Zhang L, Skinner FK. Inhibitory networks of fast-spiking interneurons generate slow population activities due to excitatory fluctuations and network multistability. J Neurosci 2012;32:9931. http://dx.doi.org/10.1523/JNEUROSCI.5446-11.2012.

[6] Wieland S, Bernardi D, Schwalger T, Lindner B. Slow fluctuations in recurrent networks of spiking neurons. Phys Rev E 2015;92:040901. http://dx.doi.org/10.1103/PhysRevE.92.040901.

[7] Litwin-Kumar A, Doiron B. Slow dynamics and high variability in balanced cortical networks with clustered connections. Nature Neurosci 2012;15:1498. http://dx.doi.org/10.1038/nn.3220.

[8] Franović I, Klinshov V. Slow rate fluctuations in a network of noisy neurons with coupling delay. Europhys Lett 2016;116:48002. http://dx.doi.org/10.1209/0295-5075/116/48002.

[9] Franović I, Klinshov V. Clustering promotes switching dynamics in networks of noisy neurons. Chaos 2018;28:023111. http://dx.doi.org/10.1063/1.5017822.

[10] Bick C, Rabinovich MI. Dynamical origin of the effective storage capacity in the brain's working memory. Phys Rev Lett 2009;103:218101. http://dx.doi.org/10.1103/PhysRevLett.103.218101.

[11] Cowan N. The magical mystery four: How is working memory capacity limited, and why? Curr Dir Psychol Sci 2010;19:51. http://dx.doi.org/10.1177/0963721409359277.

[12] Marković D, Mizrahi A, Querlioz D, Grollier J. Physics for neuromorphic computing. Nat Rev Phys 2020;2:499. http://dx.doi.org/10.1038/s42254-020-0208-2.

[13] Furber S. Large-scale neuromorphic computing systems. J Neural Eng 2016;13:051001. http://dx.doi.org/10.1088/1741-2560/13/5/051001.

[14] Schuman CD, Kulkarni SR, Parsa M, et al. Opportunities for neuromorphic computing algorithms and applications. Nat Comput Sci 2022;2:10. http://dx.doi.org/10.1038/s43588-021-00184-y.

[15] Tan H, van Dijken S. Dynamic machine vision with retinomorphic photomemristor-reservoir computing. Nature Commun 2023;14:2169. http://dx.doi.org/10.1038/s41467-023-37886-y.

[16] Marunchenko A, Kumar J, Kiligaridis A, et al. Memlumor: A luminescent memory device for photonic neuromorphic computing. 2023, http://dx.doi.org/10.48550/arXiv.2312.09170.

[17] Nakajima K, Fischer I, editors. Reservoir computing: theory, physical implementations, and applications. Natural computing series, Singapore: Springer Nature; 2021, http://dx.doi.org/10.1007/978-981-13-1687-6.

[18] Tanaka G, Yamane T, Héroux JB, Nakane R, Kanazawa N, Takeda S, Numata H, Nakano D, Hirose A. Recent advances in physical reservoir computing: A review. Neural Netw 2019;115:100. http://dx.doi.org/10.1016/j.neunet.2019.03.005.

[19] Lukoševičius M, Jaeger H. Reservoir computing approaches to recurrent neural network training. Comput Sci Rev 2009;3:127. http://dx.doi.org/10.1016/j.cosrev.2009.03.005.

[20] Maass W, Natschläger T, Markram H. Real-time computing without stable states: A new framework for neural computation based on perturbations. Neural Comput 2002;14:2531. http://dx.doi.org/10.1162/089976602760407955.

[21] Jaeger H, Haas H. Harnessing nonlinearity: Predicting chaotic systems and saving energy in wireless communication. Science 2004;304:78. http://dx.doi.org/10.1126/science.1091277.

[22] Klinshov VV, Kovalchuk AV, Franović I, Perc M, Svetec M. Rate chaos and memory lifetime in spiking neural networks. Chaos Solitons Fractals 2022;158:112011. http://dx.doi.org/10.1016/j.chaos.2022.112011.

[23] Kumar A, Irsoy O, Ondruska P, Iyyer M, Bradbury J, Gulrajani I, Zhong V, Paulus R, Socher R. Ask me anything: Dynamic memory networks for natural language processing. In: Balcan MF, Weinberger KQ, editors. Proceedings of the 33rd international conference on machine learning. Proceedings of machine learning research, vol. 48, New York, New York, USA: PMLR; 2016, p. 1378–87.

[24] Xiong C, Merity S, Socher R. Dynamic memory networks for visual and textual question answering. In: Balcan MF, Weinberger KQ, editors. Proceedings of the 33rd international conference on machine learning. Proceedings of machine learning research, vol. 48, New York, New York, USA: PMLR; 2016, p. 2397–406.

[25] Yang T, Chan AB. Learning dynamic memory networks for object tracking. In: Ferrari V, Hebert M, Sminchisescu C, Weiss Y, editors. Computer vision – ECCV 2018. Cham: Springer International Publishing; 2018, p. 153–69.

[26] Sompolinsky H, Crisanti A, Sommers HJ. Chaos in random neural networks. Phys Rev Lett 1988;61:259. http://dx.doi.org/10.1103/PhysRevLett.61.259.

[27] Ostojic S. Two types of asynchronous activity in networks of excitatory and inhibitory spiking neurons. Nature Neurosci 2014;17:594. http://dx.doi.org/10.1038/nn.3658.

[28] Mastrogiuseppe F, Ostojic S. Intrinsically-generated fluctuating activity in excitatory–inhibitory networks. PLoS Comput Biol 2017;13:e1005498. http://dx.doi.org/10.1371/journal.pcbi.1005498.

[29] Crisanti A, Sompolinsky H. Path integral approach to random neural networks. Phys Rev E 2018;98:062120. http://dx.doi.org/10.1103/PhysRevE.98.062120.

[30] Klinshov V, Franović I. Mean-field dynamics of a random neural network with noise. Phys Rev E 2015;92:062813. http://dx.doi.org/10.1103/PhysRevE.92.062813.

[31] Franović I, Maslennikov OV, Bačić I, Nekorkin VI. Mean-field dynamics of a population of stochastic map neurons. Phys Rev E 2017;96:012226. http://dx.doi.org/10.1103/PhysRevE.96.012226.

[32] Franović I, Klinshov V. Stimulus-evoked activity in clustered networks of stochastic rate-based neurons. Eur Phys J Spec Top 2018;227:1063. http://dx.doi.org/10.1140/epjst/e2018-800080-6.

[33] Luke TB, Barreto E, So P. Complete classification of the macroscopic behavior of a heterogeneous network of theta neurons. Neural Comput 2013;25:3207. http://dx.doi.org/10.1162/NECO_a_00525.

[34] Laing CR. Derivation of a neural field model from a network of theta neurons. Phys Rev E 2014;90:010901. http://dx.doi.org/10.1103/PhysRevE.90.010901.

[35] Ermentrout GB, Kopell N. Parabolic bursting in an excitable system coupled with a slow oscillation. SIAM J Appl Math 1986;46:233. http://dx.doi.org/10.1137/0146017.

[36] Ermentrout B. Type I membranes, phase resetting curves, and synchrony. Neural Comput 1996;8:979. http://dx.doi.org/10.1162/neco.1996.8.5.979.

[37] Ermentrout GB, Terman DH. Mathematical foundations of neuroscience. New York: Springer; 2010, http://dx.doi.org/10.1007/978-0-387-87708-2.

[38] Izhikevich EM. Dynamical systems in neuroscience: the geometry of excitability and bursting. Cambridge: The MIT Press; 2007.

[39] Roth A, van Rossum MCW. Modeling synapses. In: Computational modeling methods for neuroscientists. The MIT Press; 2009, http://dx.doi.org/10.7551/mitpress/9780262013277.003.0007.

[40] Watts D, Strogatz S. Collective dynamics of 'small-world' networks. Nature 1998;393:440. http://dx.doi.org/10.1038/30918.

[41] Kiselev M. Chaotic spiking neural network connectivity configuration leading to memory mechanism formation. In: Kryzhanovsky B, Dunin-Barkowski W, Redko V, Tiumentsev Y, editors. Advances in neural computation, machine learning, and cognitive research III. Cham: Springer International Publishing; 2020, p. 398.

[42] Maslennikov OV, Pugavko MM, Shchapin DS, Nekorkin VI. Nonlinear dynamics and machine learning of recurrent spiking neural networks. Phys-Usp 2022;65:1020. http://dx.doi.org/10.3367/UFNe.2021.08.039042.

[43] Jaeger H. The "echo state" approach to analysing and training recurrent neural networks-with an erratum note. Technical Report 148, Bonn, Germany: German National Research Center for Information Technology GMD; 2001.

[44] Haykin S. Adaptive filter theory. Upper Saddle River, NJ: Prentice Hal; 2002.